Cent. Eur. J. Geosci. • 4(3) • 2012 • 448-464
DOI: 10.2478/s13533-011-0077-4

VERSITA

Central European Journal of **Geosciences**

Stress analysis and tectonic trends of southern Sinai Peninsula, using potential field data analysis and anisotropy technique

Research Article

Salah Saleh[1]* and Ahmed Saleh[1]

1 *National Research institute of Astronomy and Geophysics (NRIAG), 11722 Helwan, Cairo-Egypt*

Received 15 April 2012; accepted 21 June 2012

Abstract: The aim of the present work is to evaluate the stress direction and the tectonic trends of the study area using magnetic anisotropy and potential field data interpretations (Bouguer and aeromagnetic). The specific objective of the gravity and aeromagnetic interpretation is to establish the trend and depth of the structural configuration of the basement rocks. Horizontal gradient techniques could to delineate directions of deep sources and enabled tracing several faults, lineaments and tectonic boundaries of basement rocks. The trend analysis shows N40°-50°W, N10°-20°W and N10°-20°E which may be related to the Gulf of Suez, Red Sea and Gulf of Aqaba stresses. However, Euler Deconvolution technique was applied using the aeromagnetic data to provide reliable information about penetrated source depth (100 m and ~10.0 km) and trends of the subsurface sources (principally in NW and NE directions). Moreover, representative 72 oriented rock samples have been collected from seven sites in the study area. The rock magnetic properties and magnetic anisotropy analysis have been determined for all the studied samples. The interpretation clearly defined magnetic lineation at all sites and anisotropy of magnetic susceptibility (**AMS**) parameters. The stress direction of the studied area has been evaluated using magnetic anisotropy and geophysical analysis. Generally the estimated geophysical data analysis (Bouguer and aeromagnetic) are well consistent with the AMS interpretations of this study. The results indicated that the directions of predominant faults and foliations are NW-SE (related to the Gulf of Suez and Red Sea rifting) which indicate that the main stress and tectonic trend is NE-SW, which is more predominant in southern Sinai region. Moreover, it is clear that, the studied area was affected also by less predominant sources trended in NE-SW direction, which related to the tectonic activity of Gulf of Aqaba. The least predominant is north 40°- 50° east that is probably due to the Syrian Arc system. Finally, our results are extremely coincided with the previous stress directions derived from geological, seismological and tectonic analysis in northern Red Sea rift, Gulf of Suez and Sinai regions.

Keywords: geophysics • gravity • magnetic field • interpretation • magnetic anisotropy • South Sinai • Egypt

1. Introduction

The Sinai subplate is situated at the juncture of the African, Arabian and Anatolian plates [1–4]. It includes a portion of the Eastern Mediterranean and the Levant Basin (Figure 1). These regions have been shaped since

*E-mail: salahsmm@yahoo.com

the Early Mesozoic by a series of rifting phases that formed the northeastern margin of the once continuous Afro-Arabian continent [5, 6].

The Sinai subplate is a new tectonic element that was formed as a result of a Cenozoic breakup of the Eastern Mediterranean and the Levant Basin. Many researchers studied the geology, tectonic style and kinematics of its borders: the Dead Sea left-lateral Transform (DST), which accommodates the motion between Arabia and Sinai (northeastern tip of Africa) [3, 7]; the convergent Cypriot Arc (CA) at the suture between Anatolia and Sinai [8–10]; and the Suez Rift (SR), which carries some divergence motion between Africa and Sinai [11].

While clearly these are plate boundaries, there is almost no morphologic [12], tectonic [13] or seismic [14] evidence of a northward continuation of the SR toward the CA, to completely encircle Sinai and define it as a microplate. [11], however, partly continue the SR northward, via a regional left-stepping relay beneath the Nile Delta. Recently, [15] identified an active fault belt that might correspond to an offshore extension of the SR, and suggested that this belt represents the western border of the Sinai subplate. However, its right lateral sense of motion is still a matter of debate.

Tectonics played a key role in establishing the present-day surface configuration of the Sinai micro-plate [3, 16]. The micro-plate exhibits complicated interactions at its active boundaries with Africa, Arabia, and Eurasia.

Inter-plate movements and intra-plate adjustments between crust and mantle processes have dominated Sinais geodynamic evolution. These processes are commonly associated with the rifting, uplift, and sometimes rotation that have controlled Sinais morphotectonic structures and overprinted its geomorphology in the form of topographic lineaments. An approach that detects and relates such lineaments and contacts to dominant tectonics is therefore extremely desirable to better understand the regional tectonic evolution.

Stress fields driving lithospheric tectonic deformation are largely confined to plate boundaries, but can transmit to the plate interior where they interplay over the long term with climatic/ geomorphic processes and give rise to continental domains [17–19]. The structures and orientations of these domains are largely controlled by pre-existing crustal discontinuities and stress fields [20, 21], and references therein.

The present work is an attempt to estimate the stress direction and tectonic trends of southern Sinai using different geophysical approaches and techniques. However, potential field data interpretations (Bouguer and aeromagnetic) were employed to evaluate the orientation of structuralpatterns and the main tectonic trends (faults, lineaments, tectonic boundaries) from deep to show depths along the studied area. However, magnetic anisotropy was used to estimate the stress direction according to the predominant tectonic trends affecting the study area. Therefore, tectonic activity and orientations of our study area have been well controlled using different geophysical tools (e.g., aeromagnetic and gravity datasets and magnetic anisotropy).

2. Tectonic and geological settings

The Sinai microplate (Figure 1) consists of a triangular continental crustal block locked between the major Arabia and Africa plates and the Anatolian–Aegean microplate [1, 2, 4, 22].

The microplate is bounded eastward by the Dead Sea leftlateral transform and its submerged extension in the Gulf of Aqaba.

These regions/plates have been shaped since the Early Mesozoic by a series of rifting phases that formed the northeastern margin of the Afro-Arabian continent [5, 6].

Details of the geology of Sinai are addressed by Said [23, 24], and references therein. Precambrian igneous and metamorphic basement rocks belonging to the Arabian–Nubian Shield reach an altitude of 2629 m (G. Saint Katherine) in the south and are overlain by a Phanerozoic sedimentary wedge in the north that gently dips and generally becomes more recent towards the Mediterranean coast (Figure 2).

The Dead Sea connects to the north with the left-lateral East Anatolian transform fault zone that is in continuity with the Cyprus active margin [27] and references therein that demarcates the microplates northern boundary. The Cyprean Arc is dominated by subduction and transcurrent processes along its western and eastern extents, respectively [28].

The Gulf of Suez is a confirmed segment of the microplates western boundary. Recent evidence from shallow seismic activities [16, 29] and marine geophysical data [15] confirm the northward offshore extension of the Gulf of Suez as a boundary of the microplate. Plate motion along this boundary is still amatter of debate [16]. Minor transcurrent components have been recognized in the Gulf of Suez [4, 30], their sense of motion favors a relative left-lateral strike-slip movement, which agrees with focal mechanisms of fault-plane solutions from the region [4, 13, 16, 30]. Seismological and GPS constraints reveal the dominance of slab-pull rather than ridge push forces for the motion of Sinai relative to Africa [16].

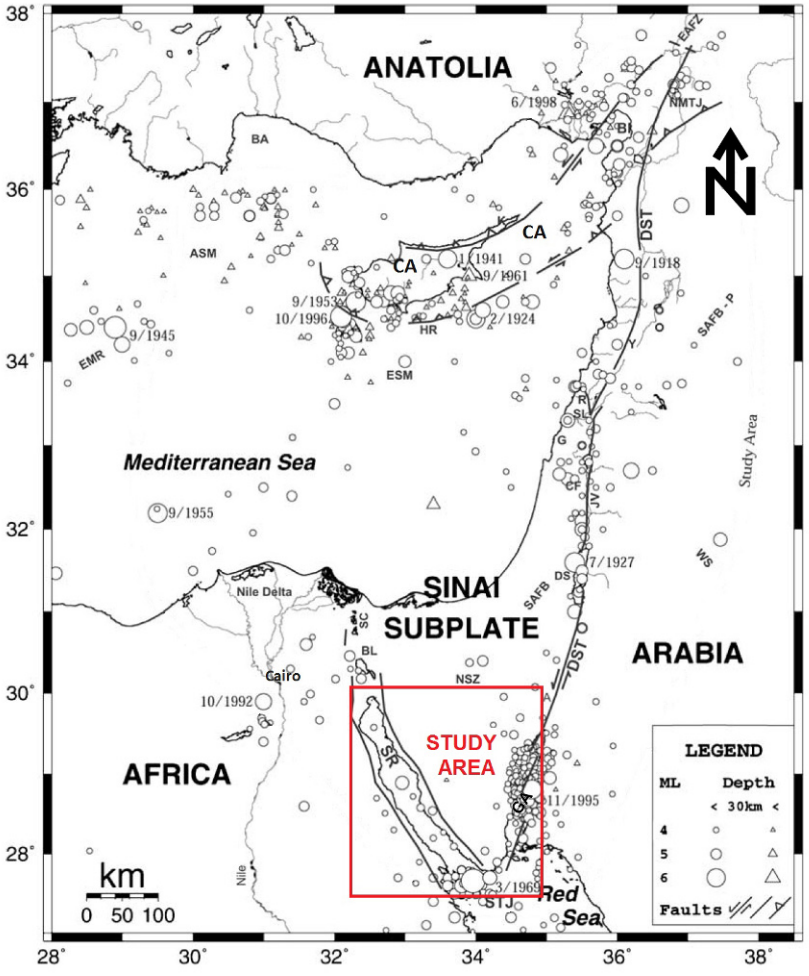

Figure 1. Seismicity and tectonics of the study area, modified after [7, 10, 14]. Most of the ML $\geq$ 5 events are concentrated along the plate borders while the smaller events are scattered around. The plates are: Africa, Arabia, Anatolia and the Sinai subplate. The plate borders are: Cypriot Arc (CA), Dead Sea Transform (DST) and Suez Rift (SR). Other geological elements and localities: ASM, Anaximander Seamount; BA, Bay of Antalya; BI, Bay of Iskenderun; BL, Bitter Lakes; CF, Carmel–Faria fault system; DS, Dead Sea; EAFZ, East Anatolian Fracture Zone; EMR, East Mediterranean Ridge; ESM, Eratosthenes Seamount; G, Galilee; GA, Gulf of Aqaba; HR, Hecteaus Rise; JV, Jordan Valley; K, Kyrenia; NMTJ, Northeast Mediterranean Triple Junction; NSZ, Negev Shear Zone; P, Palmyrides; R, Roum fault; SAFB, Syrian Arc Fold Belt (including P, Palmyrides); SC, Suez Canal; SL, South Lebanon; STJ, Sinai Triple Junction; WS, Wadi Sirhan; Y, Yammouneh bend.

Many researchers studied the geology and tectonic setting of Sinai Peninsula area [2, 3, 7, 12]

Sinai Peninsula covers a land area of approximately 61,000 m^2, highly dissected by igneous and metamorphic mountains, which rise to a height of 2675 m (Gebel Musa), forming the southern tip of the Peninsula. In the south, the exposed Pre-Cambrian igneous and metamorphic rocks form a part of the so-called Arabian-Nubian Shield which is a stable tectonic unit. The central part of Sinai Peninsula consists of sub horizontal Mesozoic and Tertiary sediments (Figure 2), creating the plateau of Gebel El Tih-Egma that represents a thin sedimentary cover, which is affected only by normal faulting (unfolded central Sinai stable foreland). These faults are distinguished into N–S to NNE–SSW, NW–SE and E–W trends. A shear zone of right lateral E–W strike slip faults with up to 2.5 km of displacement has been recognized in Central Sinai; Raqabet El-Naam right lateral wrench fault. Northward from Raqabet El-Naam right lateral wrench fault, the style of deformation becomes complex.

The topography comprises low alluvial plains, which are broken by large uplifted Mesozoic domes and anticlines, such as Gebel Yelleg, Gebel Halal and Gebel Maghara. These anticlines are of minor dimensions and are oriented in 65°N to 85°E. These anticlinal features have been described as a part of the Syrian Arc System. The Syr-

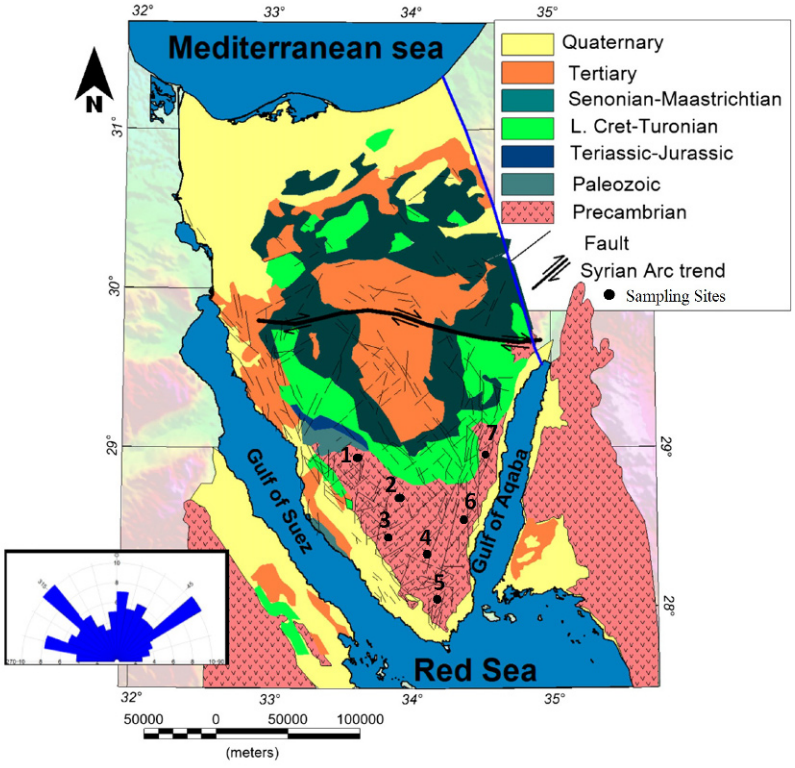

Figure 2. Schematic geological map of Sinai Peninsula of Sinai Peninsula [25, 26]. The rose diagram shows the main trends of the geologic faults in Sinai Peninsula. Gulf of Suez and Gulf of Aqaba trends can be easily recognized on the rose diagram. The black circles represent the sampling sites.

ian Arc structures attain a more northerly trend aligning themselves with the sinister Dead Sea and the Plusium line, to the east and northeast of Sinai. The area to the north of 30°N is crossed by a strong fractured zone running in NE–SW direction (Hinge Belt).

3. Geophysical data analysis and interpretation

The geophysical techniques developed in our study were applied to detecting tectonically significant lineaments, faults and tectonic boundaries characterizing the geologic structures for south Sinai and adjacent areas (Figure 2). The region is geologically and structurally complex, composed of lithologies of different types and ages and showing varying tectonic styles and trends (Figures 1 and 2). Better understanding of the kinematics and the spatial extent of the dominant tectonic trends may have implications for identifying the potential for natural resources in the area.

Many studies have addressed the repeated reactivation of the older structures by plate-scale stress fields along broad lineaments in the region [32–34].

In these studies, the evaluated structures played an important role in understanding the region's geodynamic evolution. However, these were commonly generalized sketches reviewed from interpretations of geologic observations and scarce geophysical surveys which lack spatial inter-relationships. Integrating lineaments extrapolated from various spatial data describing surface and subsurface features seems a more promising way to draw a detailed, reliable structural map of the region.

In the present work we used two grid data sets: 1) the 2-arc minute earth magnetic anomaly (nT) grid by [35, 36]. 2) Bouguer anomaly gravity data of the Egyptian General Petroleum Company [37]. Gravity and magnetic data are related to different rock attributes in the subsurface which provides a basis for joint interpretation of both kinds of data. Coinciding gravity and magnetic anomalies may suggest a common origin. Contrasting gravity and magnetic anomalies may result from erasing the crust's magnetism by heating [38] or from rocks with low magnetic contents [39]. Magnetic intensities of rocks occurring be-

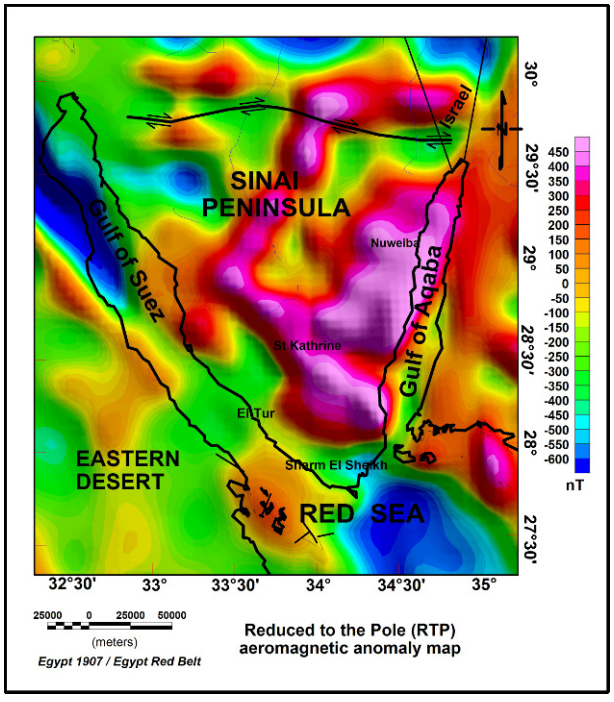

Figure 3. Reduced to the pole (RTP) aeromagnetic anomaly map of the study area, [36].

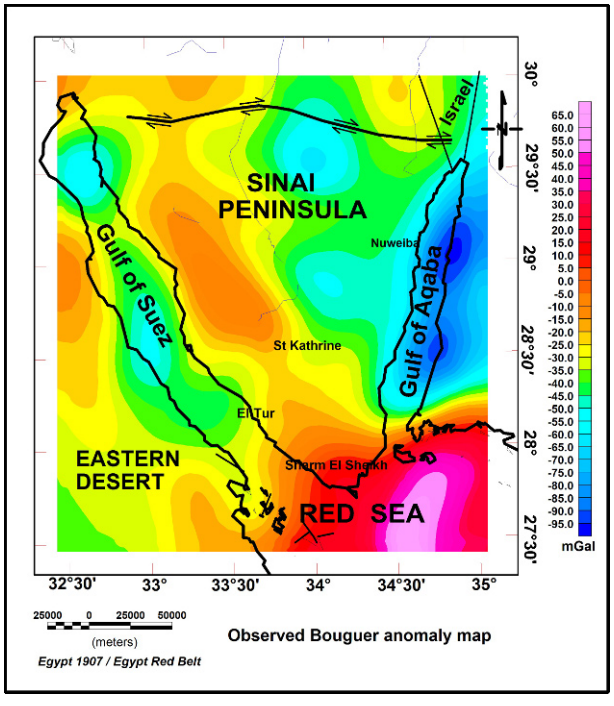

Figure 4. Bouguer anomaly map of the study area, [37].

low the Curie isotherms can provide insight into the subsurface structure and the composition of rocks in the crust. As topography, gravity, and magnetic data are mutually independent, integrated extrapolation based on all three kinds of data reduces the degree of ambiguity in surface and subsurface crustal structural modeling in the study area. Both the Reduced to the pole (RTP) aeromagnetic (Figure 3) and Bouguer anomaly maps (Figure 4) indicate that most anomalies are aligned to NW-NE, and NE-SW which may be related to the Red Sea and Gulf of Suez, and Gulf of Aqaba respectively. The negative anomalies in the central part may be due to lithology variation of the basement.

The intense magnetic anomalies aligned in E-W directions are consistent with the Tertiary and Mesozoic aged volcanic and ultramafic rocks of the region. The high amplitude anomalies lying in NW, NE and E-W directions may owe their origin to the metamorphic basement rocks found in the study area. Most of the magnetic anomalies are located in the southern and central zones of Sinai Peninsula, which is represented by Tertiary volcanic and granitic intrusions. The magnetic anomalies, which are in NW, NE and E-W directions, lie parallel to the geological and tectonic structure of the region. Therefore, it can be suggested that these magnetic anomalies derived from igneous units rising up within the fault systems, which is a result of the Neo-tectonic structure of the region (Figure 3).

The Bouguer Anomaly map (Figure 4) reveals a gravity lows in the central and southern parts. The negative anomalies in the central part (with about -40 to -50 mGal) may be due to lithologic variations of the basement layers. The alternative negative and positive anomalies along the Gulf of Suez are due to the faulted blocks or presence of different basins with different thickness of sedimentary sequences along all the area of study. Most gravity anomalies are aligned to NW and NE trends which may be related to tectonic activity of Gulf of Suez and Gulf of Aqaba respectively. Negative gravity anomalies in the Gulf of Aqaba support the idea of a shear [40]. This guides to the conclusion that the shallow parts are extending along the two gulfs and southern part of Sinai where the basement rocks are outcropping (as shown in geological map in Figure 2).

3.1. Trend analysis technique

A two lineaments map (Figure 5) was constructed from application of the second order trend analysis technique [41, 42] for the RTP aeromagnetic and Bouguer anomalies maps. These maps were subjected to statistical calculat-

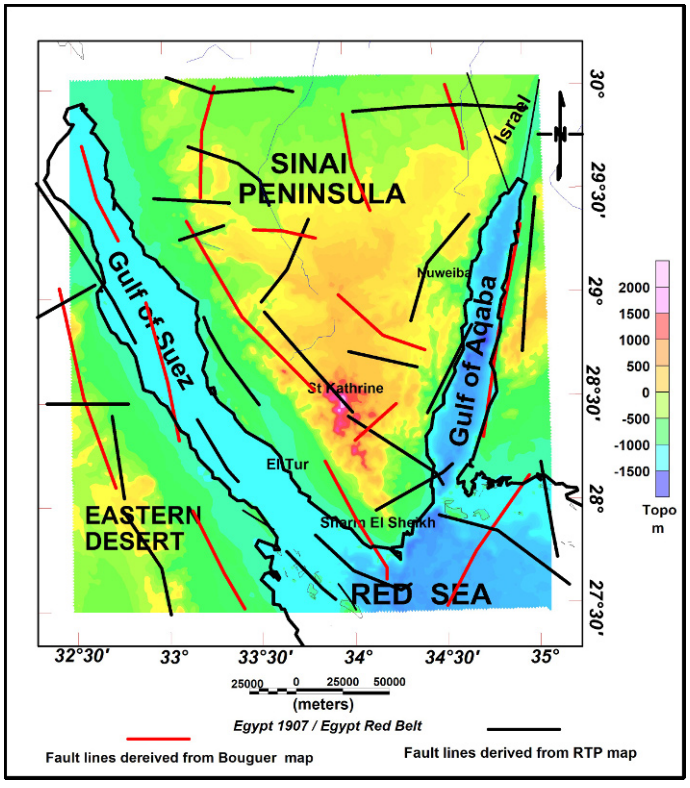

Figure 5. Tectonic lines as deduced from Bouguer anomaly (red lines) and the Reduced to the pole (RTP) aeromagnetic (black lines) maps.

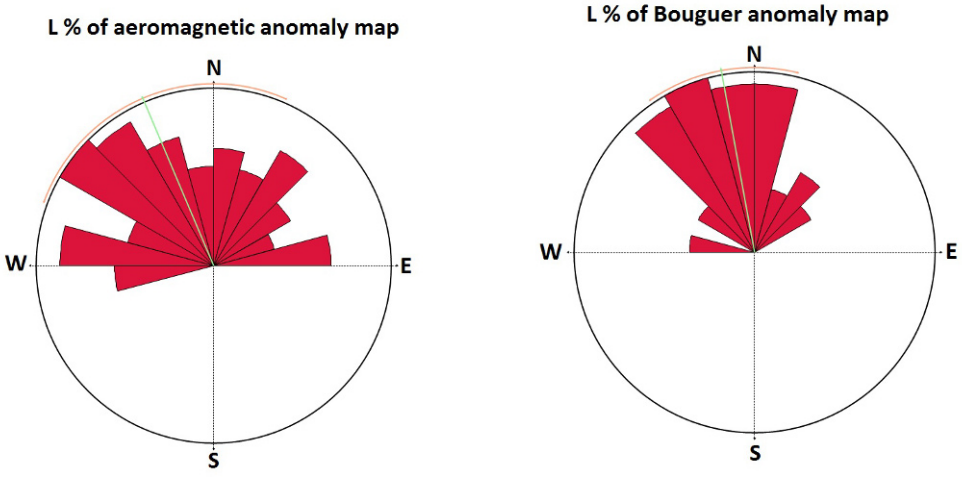

(a) (b)

Figure 6. Rose diagrams illustrate the distribution of the lengths percentage (L %) of faults against azimuth.

ing for the lengths percentages of the faults measured clockwise from the north. The deduced lineation of different directions are grouped every 10° around the north for their length percentage (L%). A statistical procedure was used to illustrate the predominant fault trends affecting the studied area. The results of azimuth distribution of both surface and subsurface elements are presented in the form of a rose diagram (Figure 6).

The results show that the most predominant direction is N40°-50°W, N10°-20°W, N40°- 50°E and N10°- 20°E trends. It is clear that the main tectonic trend is north 40°-50° west prevailing for the large scale in the Reduced to the pole aeromagnetic map. While as, the main predominant tectonic trend is north 10°-20° west existing for the large scale in the Bouguer anomaly map. This may be due to a very strong and active force resulting from the opening of the Red Sea and Gulf of Suez. The second predominant tectonic force is the north N10°- 20°E due to tectonics related to the Gulf of Aqaba. The least predominant is north 40°- 50° east that is probably due to the Syrian Arc system.

To delineate the subsurface structure of the area, we have applied two methods. These methods are horizontal gradient analysis to delineate the tectonic boundary and 3D-Eular method to estimate the structural depth values. Results of these methods, together with available geological and seismicity information are used to help in understanding the stress directions of the study area.

3.2. Horizontal gradient anomaly maps

The horizontal gradient (HG) method has been used intensively in interpretation of magnetic, gravity or psedugravity data [43, 44]. The most advantage of HG method is its least susceptible to noise in the data because it only required the calculation of the two first order horizontal derivatives of the field [45]. The amplitude of the HG of the regional RTP data of the study area was calculated in the frequency domain and is illustrated in Figures 7a.

High gradient observed around the low magnetic of the study area and is sharp like vertical boundaries of magnetic susceptibility. It indicated that the area is characterized the existence of high magnetic gradient anomalies associated with existing metasediments and volcanic intrusions.

Figure 7b shows zones of maximum of horizontal gradient data interpretation. The area may be dissected by major faults striking existence of the ENE-WSE, NW and NE directions. The most interesting result is that the locations of the major faults are well correlated with surface geological map (Figure 2) lie parallel to the lithological and geological boundaries of the region.

Full horizontal gradient map (HG) computed from Bouguer gravity data is illustrated in Figures 8. This map shows existence of steep lineaments lying to NW and NE directions. These lineaments were located on fault belts that control the tectonic of the region and lie parallel to the Suez and Aqaba gulfs. Because the steep gradients locating regions of abrupt changes in density contrast reveal the underlying fault zones, we inferred these steep lineaments determine the major tectonic zones of continental crust trending in the same directions.

3.3. 3- D Euler Deconvolution:

The 3D form of Euler's equation can be defined [46] as:

$$x\frac{\partial T}{\partial x}+y\frac{\partial T}{\partial y}+z\frac{\partial T}{\partial z}+\eta T=x_0\frac{\partial T}{\partial x}+y_0\frac{\partial T}{\partial y}+z_0\frac{\partial T}{\partial z}+\eta b \quad (1)$$

where x, y and z are the coordinates of a measuring point, x_0, y_0, and z_0 are the coordinates of the source location, b is a base level, and η is a structural index defining the anomaly attenuation rate at the observation location (e.g., $\eta = 0$ for a contact, $\eta = 1$ for the top of a vertical dike or the edge of a sill, $\eta = 2$ for the center of a horizontal or vertical cylinder, and $\eta = 3$ for the center of a magnetic sphere or a dipole, [46, 47]. By considering four or more neighboring observations at a time (an operated window), source location (x_0, y_0, z_0) and b can be computed by solving a linear system of equations generated from equation (1).

In the present study, a value of 0.5 was selected as a structural index to locate the possible magnetic contacts from the RTP magnetic data. Theoretically, a structural index of zero is an appropriate value for contact models. However, this value usually gives unstable results [48]. Figure 9a shows the 3D Euler solutions for the RTP data.

Good clustering of the solutions was obtained and showing definite magnetic trends. The solutions show several trends (NW-SE, NE-SW, E-W and N-S) and having a depths ranged between 100 m and ~10.0 km. Geologically, Sinai area is considered to be a major tectonic province controlled by trends of the Red Sea, Gulf of Suez and Gulf of Aqaba rifts [49]. Figure 9b shows a deduced structural map derived from the 3D Euler Deconvolution solution interpretation. All major tectonic features could be observed on Figure 9b. The area may be dissected by major faults striking existence of the NW and NE directions. The slight presence of structures trended in E-W

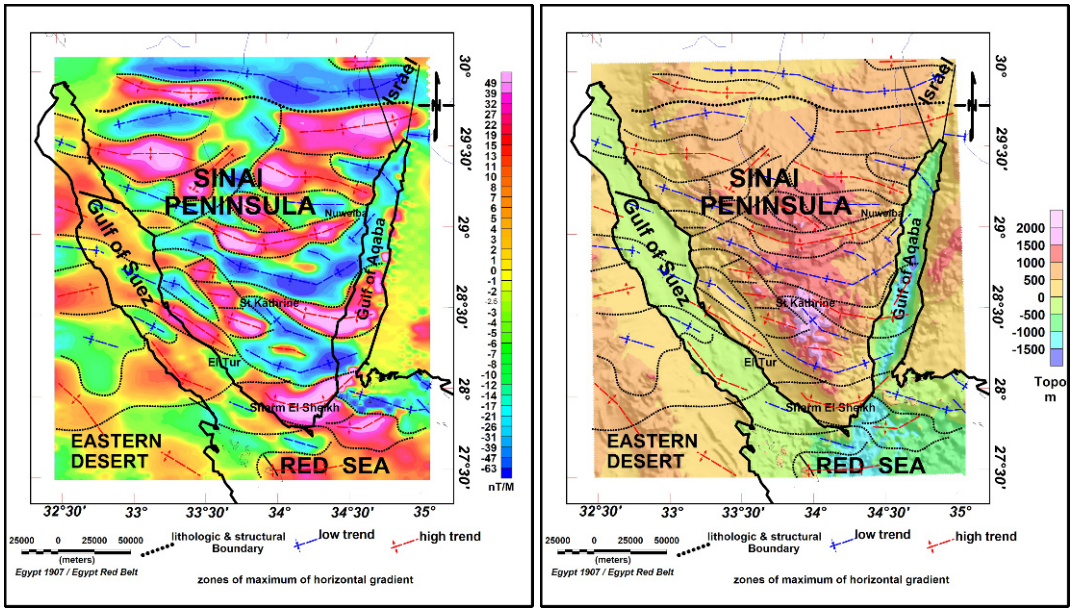

(a) (b)

Figure 7. Horizontal gradient map of the regional reduced to the pole aeromagnetic data of the study area.(a) Zones of maximum of horizontal gradient map of the reduced to the pole (RTP) aeromagnetic data of the study area. The low and high trends are plotted in blue and red lines respectively. The lithologic and structural boundaries are well defined with the dotted black lines. (b)

direction could be related to the Ragabet El-Naam E-W shear zone [50]. Other circular anomalies are observed and could be interpreted as uplifting basement or intrusion of dibasic dykes located in the region extended between Sant Kathrine and Sharm El Sheikh. The southern part of the map shows also several circular magnetic anomalies that could be related to strike-slip movements of the Gulf of Aqaba [51]. Whereas, the minor N-S of the East Africa trend system reflects the deformations of the Late and Early Paleozoic rocks

4. Magnetic Anisotropy and Rock properties

This study focuses on using the anisotropy of magnetic susceptibility (AMS) as an efficient petrofabric tool to study the direction of stress in relation to recent earthquakes. AMS was therefore called on to try to trace the assumed foliation path that these rocks may have followed during their journey soon after the occurrence of the strong earthquake until they reached their final destination. Early theoretical and laboratory studies indicate that AMS of studied rocks arises from the preferred orientation of elongate and flattened magnetic grains and could, therefore, be used as a measure of the degree and orientation of particle alignment, which in turn helps depicting palaeocurrent directions conditions [52] Hamilton and Rees 1970). Further comparative studies indicate that fabric and palaeocurrent estimated using AMS are in good agreement with those obtained from photometric, optical and other related methods [53–55].

4.1. Sampling and laboratory measurements

A total of 72 oriented samples from seven sites (as shown in Figure 2) were taken for AMS measurements using Portable Engine machine Low-field magnetic susceptibility and its anisotropy were first measured for all samples using a KLY-3S AGICO (Brno, Czech Republic) magnetic anisotropy meter (sensitivity $2\times10^{-}8$ SI), then the program ANISO [56] was used for calculation of anisotropy axes and parameters. To retrieve palaeocurrent directions from rocks of cores presently lacking orientation, magnetic remanence was measured for all samples using a three-axis 2G-Enterprises (California, USA) cryogenic magnetometer.

Rock magnetic measurements were carried out on a group of representative samples from each core to identify the type and grain size of magnetic carriers. Low-temperature magnetometry was conducted using a quantum design magnetic property measurement system

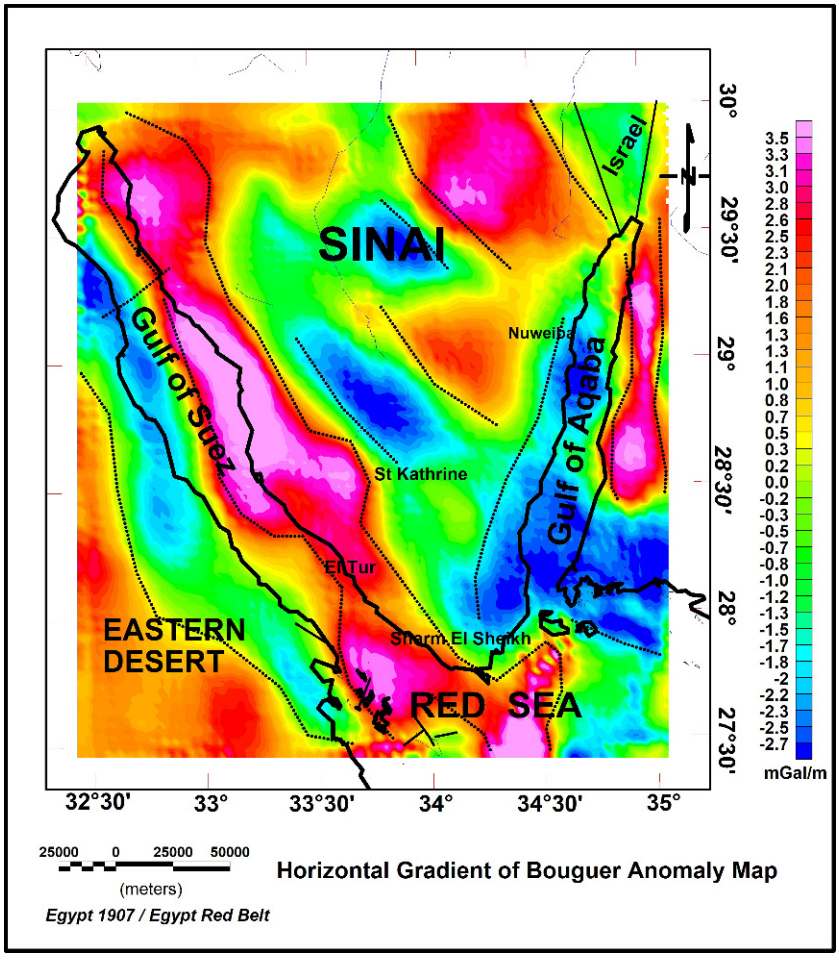

Figure 8. Horizontal gradient map of Bouguer data of the study area.

(MPMS-XL5–Quantum Design, San Diego, California, USA). First, an isothermal remanent magnetization (IRM) of 2.5 T was imparted to the sample at 300 K then magnetization changes with temperature were measured by cycling the temperature between 300 and 6 K in a nearly zero field. Next, an IRM of 2.5 T was given to the sample after being cooled down to 6 K in a zero field then the thermal demagnetization of the IRM up to 250 or 300 K was measured. An IRM acquisition experiment was also performed using a pulse magnetizer where an IRM of 0.3 T was imparted on a sample in the opposite direction after an IRM of 2.5 T was given. The S ratio (S−0.3T) was then calculated according to the definition of [57]. Finally, magnetic hysteresis loops were measured on representative dried samples using a vibrating sample magnetometer (Molspin VSM)–Molspin Ltd, Newcastle, UK to determine the dominant magnetic grain size.

4.2. Analysis and results

4.2.1. Magnetic mineralogy and grain size

Magnetization curves during zero-field low-temperature cycling of IRM imparted at 300 K show that magnetization during cooling down was larger than during warming up above approximately 100 K (Figure 10). This magnetization loss was caused as a result of passing through the magnetic isotropic point of magnetite (TI) and the Verwey transition known to occur at 110–120 K for pure magnetite [58]. The temperature TI is about 130 K for pure magnetite and is often lowered by substitution of Ti4+ [59]. Calculated S ratios (S−0.3T) from IRM acquisition experiments also support the assumption that magnetite is the principal magnetic carrier. The ratios are very high and uniform, ranging from 0.98 to 0.99, indicating the predominance of low-coercivity magnetic minerals such as magnetite. Magnetic domain state was estimated

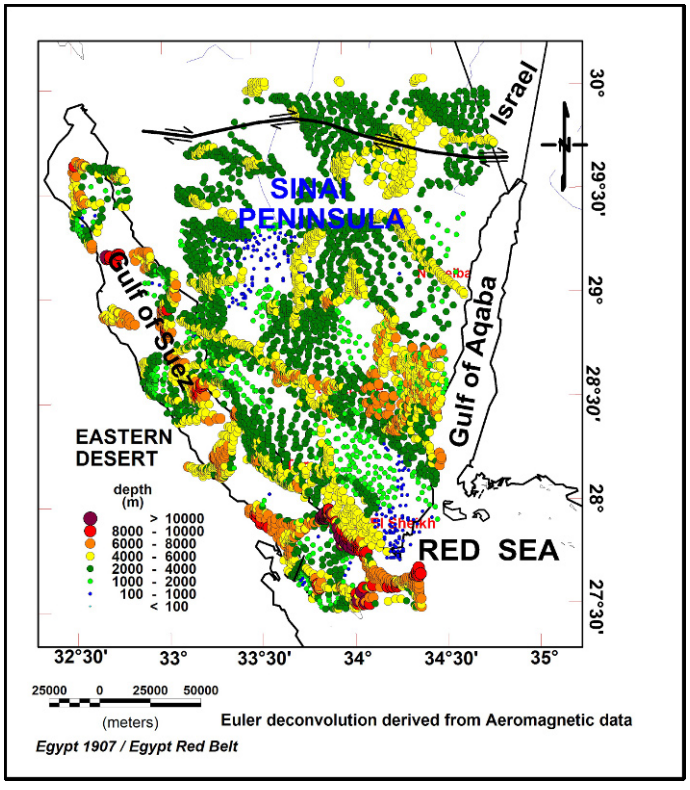

(a)

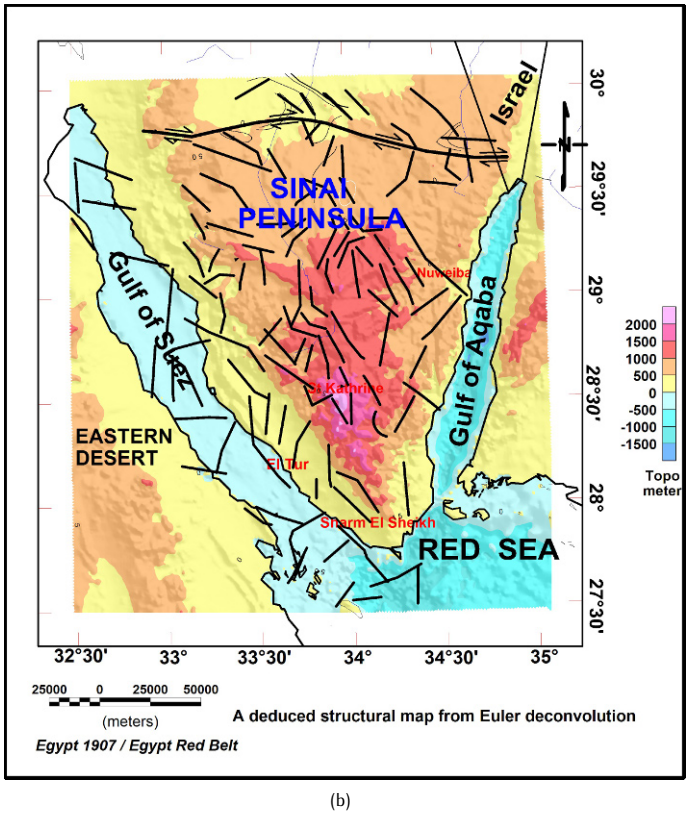

(b)

Figure 9. 3D Euler Deconvolution solution from reduced to the pole aeromagnetic data of the study area. (a) A deduced structural map derived from 3D Euler Deconvolution solution of the aeromagnetic data. (b)

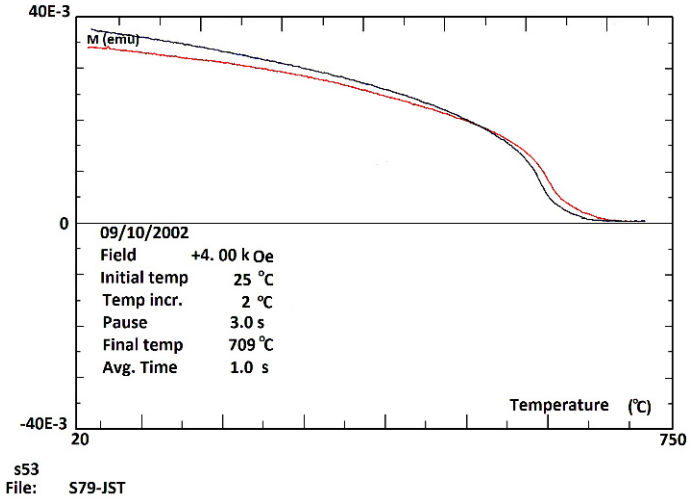

Figure 10. Thermomagnetic (JS-T) curve of one samples from Granite and is typical for pure magnetite.

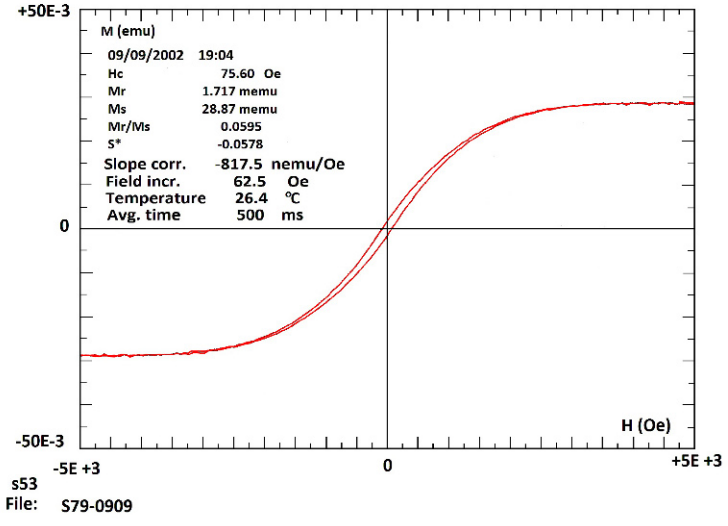

Figure 11. Hysteresis loop for one sample from granite.

from the hysteresis parameters: the ratio of saturation magnetization to saturation remanence (Mrs/Ms) and the ratio of coercivity of remanence to coercivity (Bcr/Bc). On the plot of Mrs/Ms versus Bcr/Bc [60], most samples lie within the pseudo-single domain range (Figure 11).

4.2.2. Anisotropy of magnetic susceptibility

The AMS (magnetic fabric) can be approximated by a second-rank tensor that can be represented as a triaxial ellipsoid whose magnitude and direction are described by the principal susceptibilities $K1 \geq K2 \geq K3$, which are the maximum, intermediate and minimum susceptibility axes, respectively [61, 62]. The AMS ellipsoid is described in terms of the magnetic foliation plane (K1−K2), which is normal to K3 and the magnetic lineation within the fo-

liation plane and lies along the K1-axis. The degree of grain alignment is expressed through the anisotropy magnitude. Many AMS parameters (Pj, L, F, q) have been proposed and used variously to describe the magnetic fabric of rocks. In this study we followed the recommendations of [62, 64]. Studies of Diorite rocks have demonstrated that a primary fabric induced by stress should posses a well-defined magnetic foliation in or near the bedding plane and a pole to bedding (K3) that is close to vertical. Lineation is usually subordinate to foliation with low anisotropy and uniform q values that are <0.7. In the present study, q values <0.7 together with K3 directions lying within 25°of the vertical were considered indicative of a primary fabric that can provide credible records of palaeocurrent direction and depositional conditions [52].

Magnetic susceptibility and its anisotropy were measured for all samples from the seven sites. It reflects changes in concentration of magnetic minerals. It is moderate with values generally higher than 10−6 SI indicating a predominant ferromagnetic contribution [64]. The two sets of measurements from the five sites show identical magnetic susceptibility behavior reflecting measurement consistency and within-site homogenous distribution of magnetic minerals. The highest recorded magnetic susceptibility values are obtained for granite from the samples at site 3, while the lowest values are from granite of the samples at site 5. Such anomalous fabrics are attributed to either natural or induced deformation as a result of coring and subsampling disturbances commonly reported for Rocks [65–67].

4.2.3. Palaeocurrent estimated from AMS

The palaeomagnetically oriented stereographic plots of the principal K1 and K3 susceptibility axes that satisfy the criteria for a primary fabric at each site (Figure 12) show that there is a clear grouping of K3 axes near the vertical in granite from all cores: reflecting a well developed near-horizontal magnetic foliation throughout the studied parts of the granite. These alignments are brought up more clearly in the associated rose diagram in Figure 12. Such good alignment of long grain axes reflects preferred palaeocurrent directions along these trends. Moreover, observable preferred grain imbrications can also be seen at the three multiple core sites (Figure 12) enabling absolute palaeocurrent direction determination.

It is noticeable that although plots from the majority of all samples confirm the presence of an axial NW–SE magnetic lineation, those from the other two sites show slight NE–SW and E-W foliation direction (Figure 13). The direction of the major stress in the study area considered perpendicular to the major foliation direction (NE-SW).

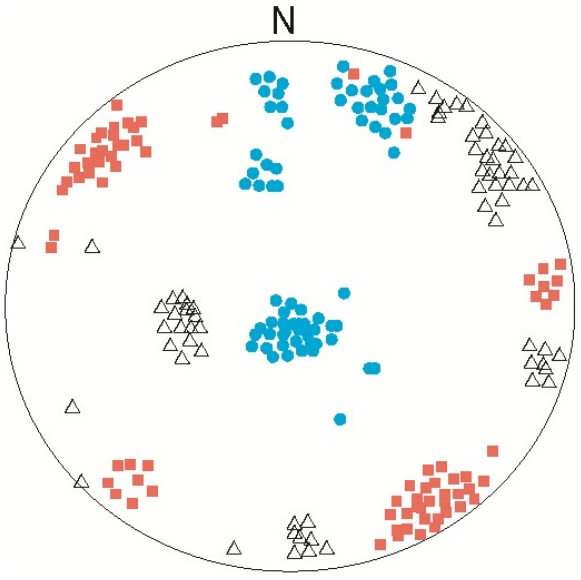

Figure 12. Principal directions of the anisotropy of magnetic susceptibility of low field, induced magnetization (AMS). Stereographic projections of K1 (Squares), K2 (Triangle) and K3 (Circles) axes and rose diagrams showing azimuthally distribution of K1 axes from Primary fabric carrying granite in seven sites. The maximum axes are sub parallel to the mineral lineation which take NW-SE direction.

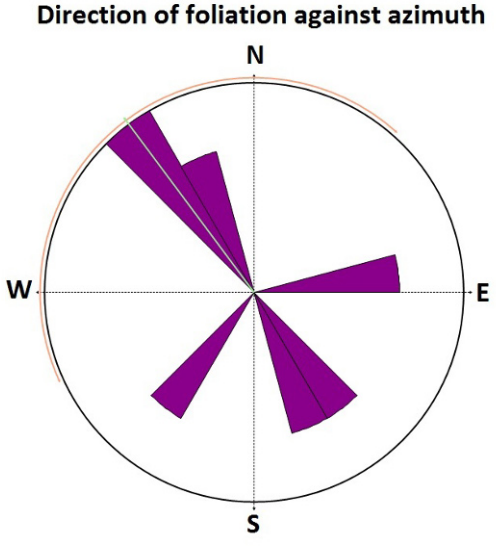

Figure 13. Rose diagrams illustrate the direction of foliation against azimuth.

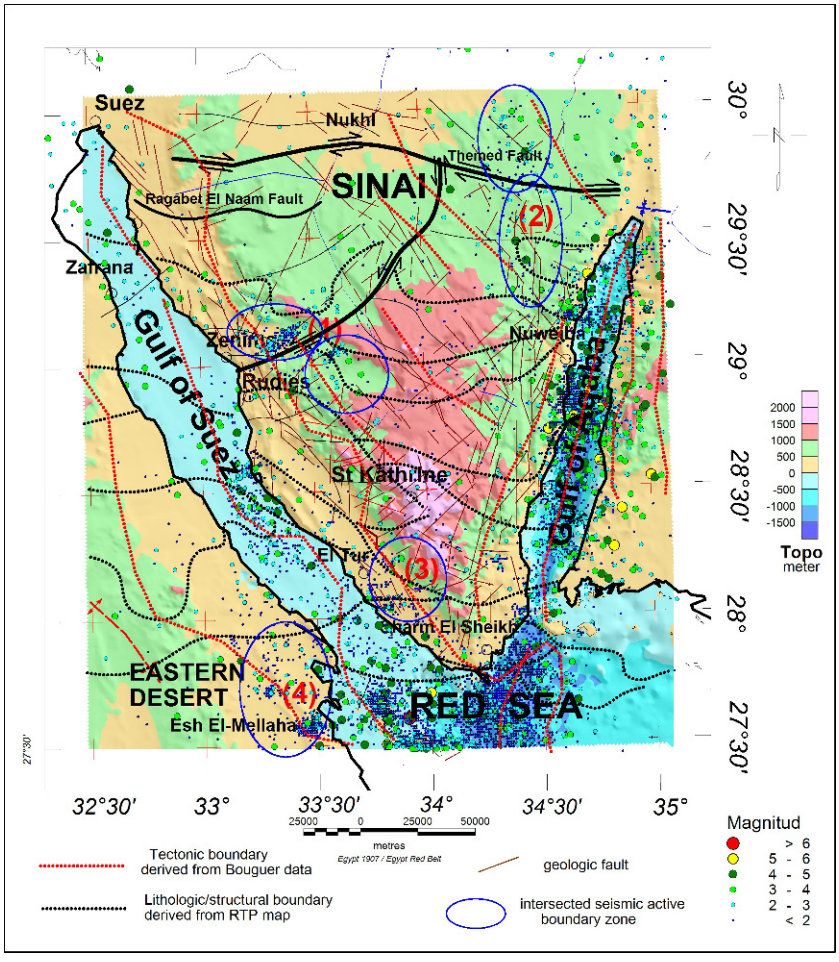

Figure 14. Geophysical-derived segments (faults and tectonic boundaries) with earthquake epicenters overlying the estimated tectonic boundary map. Note the foci of epicenters, derived from Egyptian National Seismic Network, [81] are located where the boundary zones are meeting and intersected together (elliptical blue circles). Also, note the location of seismic zone which extended from the central G. of Suez (between Zenima and Rudies) to the northeast cutting Themed fault, located along the intersection of NE fault zone.

5. Discussion and conclusions

According to microtectonic analyses [68, 69], the shortening during the development of the Cretaceous/Paleocene structures resulted from E–W to WNW–ESE horizontal compression where this was generally NNW–SSE directed in the Western Desert, shifting progressively to NW in Sinai and nearly E–W in neighboring regions to the east [70]. This eastward increase in the shortening along the Tethyan margins [71] is synchronous with counterclockwise rotational northward drift of the African–Arabian plate and its increased collisional coupling with the Eurasian plate [72, 73].

Depending on previous studies [25, 26], the predominant tectonic trends and structural styles, (as shown the rose diagram in Figure 2) are in NW and NE directions which well coincided with the results of the present work. Moreover, focal mechanism solutions and maximum shear analysis show that extensional strains and normal faulting are predominant in the Gulf of Suez province and compressional strains with left lateral strike slip styles prevail in the Gulf of Aqaba province [74–78].

The detected structural features and their trends correspond well with those derived from the Anisotropy data. This correspondence can be supported further by the intimate association of these features with regional deep-crustal shear zones and boundaries derived from geophysical data (Figure 14). Recent seismic activity has been focused along these shear zones and at their intersections, within and at the boundaries of the plate. Most of the events that played key roles in developing the configuration of NE Africa and the Sinai are associated with worldwide plate reorganizations [79, 80].

This study was carried out using different geophysical tools (aeromagnetic, Bouguer, magnetic anisotropy and seismological data). The data were analyzed using the most advanced and suitable techniques. The results of tectonic trend analysis indicate that most of the predominant directions are north 40°-50° west direction that related to Gulf of Suez and Red Sea tectonics, however NE is less predominant that related to Gulf of Aqaba tectonics. Whereas, the least predominant tectonic direction (E-W) is related to the Syrian arc system. The application of Euler Deconvolution with a suitable sliding window to estimate the position of the subsurface intruded magnetic bodies indicates that the depth to these bodies ranges from 100 m to about 10 km. Good clustering of the solutions obtained show several trends which are trending in NW-SE, NE-SW, E-W and N-S directions. Furthermore, application of the spectral analysis method confirms the result deduced by the Euler deconvolution technique. Nevertheless, the horizontal gradient map prints out a complete view for the geometry tectonic boundaries with their relation to seismic activity distributions.

The results indicate that the structures of the area are related to Gulf of Suez, and Red Sea tectonics (NW trend) and Gulf of Aqaba (NE trend).

The geophysical-derived segments map (Figure 14) show that the foci of epicenters are of scattered distribution in most area of south Sinai, i.e., the south Sinai shield. They are concentrated in seismic segments in three areas, (where the boundary zones dotted in blue circles are meet and intersected together).

-On the eastern side of the Gulf of Suez with short length segments trending in the NE-SW direction and nearly perpendicular to the Gulf of Suez (segment 1).

-North of the Gulf of Aqaba exhibiting a shear zone of NNW-SSE cutting Themed fault segment in central Sinai (segment 2).

-On the southern side of G. of Suez south El Tur, a shear zone of E-W direction (segment 3)

These three seismic zones are well correlated with the fault trends and boundary zones of the subsurface structures (tectonics of the basement rocks) derived by geophysical data analysis. Moreover, a fourth shear zone was observed trended in NW direction on Esh El Mellaha at the entrance of Gulf of Suez along the Eastern Desert side (segment 4). Finally, we can conclude that, the recent tectonic activity along south Sinai is mostly controlled by the Gulf of Suez and Red Sea rifting which trended in NW direction.

Furthermore, magnetomineralogical investigations including low-temperature magnetometry, magnetic hysteresis loops and isothermal remnant magnetization (IRM) acquisition experiments indicate that pseudo-single domain (magnetite), is the principal magnetic carrier. Clearly defined magnetic lineation was observed at the majority of all sites (nearly NW-SE) and is considered to reflect the palaeocurrent direction. The direction of the stress in the study area considered perpendicular to this direction.

Acknowledgments

We would like to thank anonymous reviewers for their through critical and constructive comments that greatly contributed to improving our manuscript.

References

[1] McKenzie, D.P., Plate tectonics of the Mediterranean region. *Nature*, 1970, 226, 239–243, doi: 10.1038/226239a0

[2] McKenzie, D.P., Davies, D., Molnar, P., Plate tectonics of the Red Sea and East Africa, *Nature*, 1970, 226, 243–248

[3] Ben-Menahem, A., Nur, A., Vered, M., Tectonics, seismicity and structure of the Afro-Euroasian junction—the breaking of an incoherent plate, *Phys. Earth planet. Inter.*, 1976, 12, 1–50

[4] Joffe, S., Garfunkel, Z., Plate kinematics of the Circum Red Sea—a re-evaluation. *Tectonophysics*, 1987, 141, 5–22

[5] Ben-Avraham, Z., Ginzburg, A., Displaced terranes and crustal evolution of the Levant and the Eastern-Mediterranean. *Tectonics*, 1990, 9, 613–622

[6] Garfunkel, Z., Constrains on the origin and history of the Eastern Mediterranean basin. *Tectonophysics*, 1998, 298, 5–35

[7] Garfunkel, Z., Zak, Y., Freund, R., Active faulting in the Dead Sea rift. *Tectonophysics*, 1981, 80, 1–26

[8] McKenzie, D., Active tectonics of the Mediterranean region. *Geophys. J. R. Astr. Soc.*, 1972, 30, 109–185

[9] Kempler, D., Ben-Avraham, Z., The tectonic evolution of the Cyprean arc. *Ann. Tectonicae*, 1987, 1, 58–71

[10] Kempler, D., Garfunkel, Z., The northeast Mediterranean triple junction from a plate kinematics point of view. *Bull. Tech. Univ. Istanbul*, 199, 144, 203–232

[11] Bosworth,W., McClay, K., Structural and stratigraphic evolution of the Gulf of Suez rift, Egypt: a synthesis, in Peri-Tethys Memoir 6: Peri- Tethyan rift/wrench basins and passive margins. Memoires du Museum

National d'Histoire Naturalle de Paris, 2001, 186, 567–606

[12] Hall, J.K.,. Bathymetric chart of the Eastern Mediterranean, Isr. Geol. Surv. 1 Map, 1994, scale 1: 625 000

[13] Garfunkel, Z., Bartov, Y., The tectonics of the Suez Rift. *Israel Geol. Surv. Bull.*, 1977, 71, 44

[14] Salamon, A., Hofstetter, A., Garfunkel, Z., Ron, H., Seismicity of the eastern Mediterranean region: perspective from the Sinai subplate. *Tectonophysics*, 1996, 263, 293–305

[15] Mascle, J., Benkhelil, J., Bellaiche, G., Zitter, T., Woodside, J., Loncke, L., Prismed II Scientific Party, Marine geologic evidence for a Levantine–Sinai Plate, a new piece of the Mediterranean puzzle. *Geology*, 2000, 28, 779–782

[16] Badawy, A., Mohamed, A.M.S., Abu-Ali, N., Seismological and GPS constraints on Sinai sub-plate motion along the Suez rift. *Stud. Geophys. Geod.*, 2008, 52 (3), 397–412

[17] Burbank, D.W., Anderson, R.S., Tectonic Geomorphology. Blackwell Sciences, Inc, Malden, 2001

[18] Roessner, S., Strecker, M., Late Cenozoic tectonics and denudation in the CentralKenya Rift: quantification of long term denudation rates. *Tectonophysics*, 1997, 278, 83-94

[19] Summerfield, M.A. (Ed.), Geomorphology and Global Tectonics. John Wiley and Sons, Indianapolis, E.E.U.U., 2000

[20] Cloetingh, S., Cornu, T., Ziegler, P.A., Beekman, F., Environmental Tectonics (ENTEC) Working Group, Neotectonics and intraplate continental topography of the northern Alpine Foreland. *Earth Sci. Rev.* 2006, 74, 127–196

[21] Cloetingh, Thybo, H., Faccenna, C., Topo-Europe: studying continental topography and Deep Earth—surface processes in 4D. *Tectonophysics*, 2009, 474, 4–32

[22] Le Pichon, X., Francheteau, J., A plate tectonic analysis of the Red Sea Gulf of Aden area. *Tectonophysics*, 1987, 46, 369–406

[23] Said, R., The Geology of Egypt. Elsevier, Netherlands, 1962

[24] Said, R., The Geology of Egypt. A. A. Balkema Publishers, Rotterdam, Netherlands, 1990

[25] Ginzburg, A., Makris, J., Fuches, K., Prodehl, C., Kaminsky, W., Amitai, U., A seismic study of the crust and upper mantle of the Jordan-Dead Sea rift and their transition toward the Mediterranean Sea. *J. Geophys. Res.* 1979, 84, 1569–1582

[26] Neev, D., Tectonic evolution of the Middle East and the Levantine Basin (easternmost Mediterranean). *Geology*, 1975, 3, 683–686

[27] Ben Avraham, Z., Tibor, G., Limonov, A.F., Leybov, M.B., Ivanov, M.K., Tokarev, M.Y., Woodside, J.M., Structure and tectonics of the eastern Cyprean arc. *Mar. Pet. Geol.*, 1995, 12, 263–271

[28] Wdowinski, S., Z. BenAvraham, R. Arvidsson and G. Ekström, Seismotectonics of the Cyprian Arc, *Geophys. J. Int.*, 2006, 164, 176181, doi: 10.1111/j.1365246X. 2005.02737.x

[29] Kebeasy, R., Seismicity. In: Said, R. (Ed.), The Geology of Egypt. Balkema, Rotterdam, 1990, 51–59

[30] Abdel-Gawad, M., New evidence of transcurrent movements in the Red Sea areas and petroleum implications. *Am. Assoc. Pet. Geol. Bull.*, 1969, 53, 1466–1479

[31] McKenzie, D.P., Surface deformation, gravity anomalies and convection. GJRAS, 1977, 48, 211–238

[32] Guiraud, R., Bellion, Y., Late carboniferous to recent geodynamic evolution of the West Gondwanian cratonic Tethyan margins. In: Nairn, A., Dercourt, J., Vrielynck, B. (Eds.), The Ocean Basins and Margins, 8: The Tethys Ocean. Plenum Press, New York, NY, 1995, 101–124

[33] Guiraud, R., Bosworth, W., Phanerozoic geodynamic evolution of northeastern Africa and the northwestern Arabian platform. *Tectonophysics*, 1999, 315, 73–108

[34] Bumby, A.J., Guiraud, R., The geodynamic setting of the Phanerozoic basins of Africa. *J. Afr. Earth Sci.*, 2005, 43, 1–12

[35] Maus, S., Sazonova, T., Hemant, K., Fairhead, J.D., Ravat, D., National geophysical data center candidate for the world digital magnetic anomaly map. *Geochemistry, Geophysics, Geosystems,* 2007, 8 (Q06017). doi:10.1029/ 2007GC001643.

[36] Maus, S., Barckhausen, U., Berkenbosch, H., Bournas, N., Brozena, J., Childers, V., Dostaler, F., Fairhead, J.D., Finn, C., von Frese, R.R.B., Gaina, C., Golynsky, S., Kucks, R., Lühr, H., Milligan, P., Mogren, S., Müller, D., Olesen, O., Pilkington, M., Saltus, R., Schreckenberger, B., Thébault, E., Caratori Tontini, F., EMAG2: A 2-arc-minute resolution Earth Magnetic Anomaly Grid compiled from satellite, airborne and marine magnetic measurements. *Geochemistry, Geophysics, Geosystems*, 2009, 10 (Q08005). doi:10.1029/2009GC002471

[37] Egyptian General Petroleum Corporation, A. S.R.T., Bouguer gravity map of Egypt, (scale 1:500:000), 1980

[38] Milbury, A.E.C., Smrekar, S.E., Raymond, C.A., Schubert, G., Lithospheric structure in the east region of Mars'dichotomy boundary. *Planetary and Space Sci-*

ence, 2007, 55, 280–288

[39] Fichler, C., Rundhovde, E., Olesen, O., Saether, B.M., Ruelatten, H., Lundin, E., Dore, A.G., Regional tectonic interpretation of image enhanced gravity and magnetic data covering the mid-Norweigian shelf and adjacent mainland. *Tectonophysics*, 1999, 306, 183–197

[40] Allan, T. D., Magnetic and gravity field over the Red Sea. *Phil. Trans. Roy. Soc. Lond. A.*, 1970, 267, 153-180

[41] Grant, F.S. and West G.F., Interpretation Theory in Applied Geophysics, McGraw-Hill Book Co., New York, 1965, 179-191

[42] Parasnis, D.S., Principles of Applied Geophysics (Chapman and Hall Publisher, London, U.K.), 5th edition, 1997, 21-25

[43] Cordell, L., Grauch, V. J., Mapping basement magnetization zones from Aeromagnetic data in San Juan Basin, New Mexico, in Hinze, W. J., Ed. The Utility of regional gravity and magnetic anomaly maps. *Sot. Explor. Geophys.*, 1985, 181-197

[44] Blakely, R. J., Potential theory in gravity and magnetic applications: Cambridge Univ. Press, 1995

[45] Phillips, J. D., Processing and Interpretation of Aeromagnetic Data for the Santa Cruz Basin-Patagonia Mountains Area, South-Central Arizona, USGS, 1998 Open File Report 02-98. Available online at: http://geopubs.wr.usgs.gov/open-file/of02-98/

[46] Reid, A.B., Allsop, J.M., Granser, H., Millett, A.J., Somerton, I.W., Magnetic interpretation in three dimensions using Euler Deconvolution. *Geophysics,* 1990, 55, 80-91

[47] Thompson, D.T., EULDPH – A new technique for making computer-assisted depth estimates from magnetic data. *Geophysics*, 1982, 47, 31-37

[48] Barbosa, V.C.F., Silva, J.B.C., and Medeiros, W.E., Stability analysis and improvement of structural index estimation in Euler Deconvolution. *Geophys,* 1999, 64, 48-60.

[49] Abu Al-Izz, M.S., Landforms of Egypt, Dar- Al-Maaref, Cairo, Egypt, 1971, 281p.

[50] Ghazala, H.,. Structural interpretation of the Bouguer and aeromagnetic anomalies in central Sinai. *Journal of African Earth Sciences*, 1994, 19, 35--42

[51] Ben-Avraham, Z., Structural framework of the gulf of Elat (Aqaba), northern Red Sea. *J. Geophys. Res.*, 1985, 90, 703–726

[52] Hamilton, N., Rees, A.I., Magnetic fabric of sediments from the Shelf at La Jolla (California), Mar. Geol., 1970, 9, M6–M11

[53] Taira, A., Lienert, B.R., The comparative reliability of magnetic, photometric and microscopic methods of determining the orientations of sedimentary grains. *J. Sed. Petrol.*, 1979, 49, 759–772

[54] Taira, A., Niitsuma,N., Turbidite sedimentation in the Nankai Trough as interpreted from magnetic fabric, grain size and detrital modal analyses, in Init. Reports DSDP, 1986, 87, 611–632, U.S. Govt. Printing Office, Washington

[55] Schieber, J., Ellwood, B.B., The coincidence of macroscopic paleocurrent indicators and magnetic lineation in shales from the Precambrian belt basin, *J. Sed. Petrol.,* 1988, 58, 830–835

[56] Jelinek, V., Characterization of magnetic fabric of rocks, *Tectonophysics*, 1981, 79, 63–567

[57] Bloemendal, J., King, J.W., Hall, F.R., Doh, S. J., Rock magnetism of Late Neogene and Pleistocene deep-sea sediments: relationship to sediment source, diagenetic processes, and sediment lithology. *J. Geophys. Res.,* 1992, 97, 4361–4375

[58] Verwey, E.J.W., Electronic conduction of magnetite (Fe3O4) and its transition point at low temperature. Nature, 1939, 144, 327–328

[59] Dunlop, D.J., Ozdemir, O., Rock magnetism, fundamentals and frontiers, Cambridge Univ. Press, 1997

[60] Day, R., Fuller, M., Schmidt, V. A., Hysteresis properties of Titanomagnetites: grain-size and compositional dependence. *Phys. Earth planet. Int.*, 1977, 13, 260–267

[61] Hrouda, F., Magnetic anisotropy of rocks and its application in geology and geophysics. *Geophys. Surv.*, 1982, 5, 37–82

[62] Tarling, D.H., Hrouda, F., The Magnetic Anisotropy of Rocks, Chapman and Hall, London, 1993

[63] Ellwood, B.B., Hrouda, F., Wagner, J.-J., Symposia on magnetic fabrics: introductory comments. *Phys. Earth planet. Int.,* 1988, 51, pp. 249–252

[64] Rochette, P., Jackson, M., Aubourg, C., Rock magnetism and the interpretation of anisotropy of magnetic susceptibility. *Rev. Geophys.*, 1992, 30, 209–226

[65] Rees, A.I., Frederick, D., The magnetic fabric of samples from the Deep Sea Drilling Project, Legs I-IV. *J. Sed. Petrol.*, 1974, 44, 655–662

[66] Kent, D.V., Lowrie, W., On the magnetic susceptibility anisotropy of deep-sea sediments. *Earth planet. Sci. Lett.*, 1975, 28, 1–12

[67] Rosenbaum, J., Reynolds, R., Smoot, J., Meyer, R., Anisotropy of magnetic susceptibility as a tool for recognizing core deformation: reevaluation of the paleomagnetic record of Pleistocene sediments from drill hole OL-92, Owens Lake, California. *Earth planet. Sci. Lett.,* 2000, 178, 415–424

[68] Eyal, Y., Reches, Z., Tectonic analysis of the Dead Sea Rift region since the Late Cretaceous based on

mesostructures. *Tectonics*, 1983, 2, 167–185

[69] Letouzey, J., Tremolieres, P., Paleo-Stress Fields around the Mediterranean since the Mesozoic from Microtectonics. Comparison with Plate Tectonic Data. *Rock Mech. Supply*, 1980, 9, 173–192

[70] Sehim, A., Cretaceous tectonics in Egypt. *Egypt. J. Geol.* 1993, 37, 335–372

[71] Guiraud, R., Bosworth, W., Senonian basin inversion and rejuvenation of rifting in Africa and Arabia: synthesis and implications to plate-scale tectonics. *Tectonophysics*, 1997, 282, 39–82

[72] Le Pichon, X., Bergerat, E., Roulet, M.-J, Plate kinematics and tectonics leading to the Alpine belt formation; a new analysis. *Geol. Soc. Am. Spec. Pap.*, 1988, 218, 111–131

[73] Ziegler, P.A., Geological Atlas of Western and Central Europe, Shell International Petroleum Mij. B.V., distributed by Geological Society, London, 2nd. Ed. Publishing House, Bath, 1990

[74] Badawy, A., Horváth, F., Recent stress field of the Sinai subplate region. *Tectonophysics*, 1999, 304, 385–403

[75] Badawy, A., Horváth, F., Seismicity of the Sinai subplate region: kinematic implications. *J. Geodyn.* 1999, 27, 451–468

[76] Badawy, A., Horváth, F., The Sinai sub-plate and tectonic evolution of the northern Red Sea region, 1999c, *Geodynamics,* 27, 433–450

[77] El-Fiky, G., GPS-derived velocity and crustal strain field in the Suez-Sinai Area, Egypt. *Bull. Earthquake Res. Inst. Univ. Tokyo*, 2005, 80, 73–86

[78] Mahmoud, S., Seismicity and GPS-derived crustal deformation in Egypt, *Geodynamics*, 2003, 35, 333-352

[79] Bunge, H.-P., Richards, M.A., Baumgardner, J.R., Mantle circulation models with sequential data assimilation: inferring present-day mantle structure from platemotion histories. *Philos. Trans. R. Soc. Ser.*, 2002, A 360, 2545–2567

[80] Scotese, R.C., Gahagan, L., Larson, R.L., Plate tectonic reconstructions of the Cretaceous and Cenozoic ocean basins. *Tectonophysics*, 1988, 155, 27–48

[81] Egyptian National Seismic Network (ENSN), Local Earthquakes recorded in Egypt from 1st Jun. to-31 Dec. 2009. *Bulletin of National Research Institute of Astronomy and Geophysics (NRIAG), Helwan, Egypt*, 2010